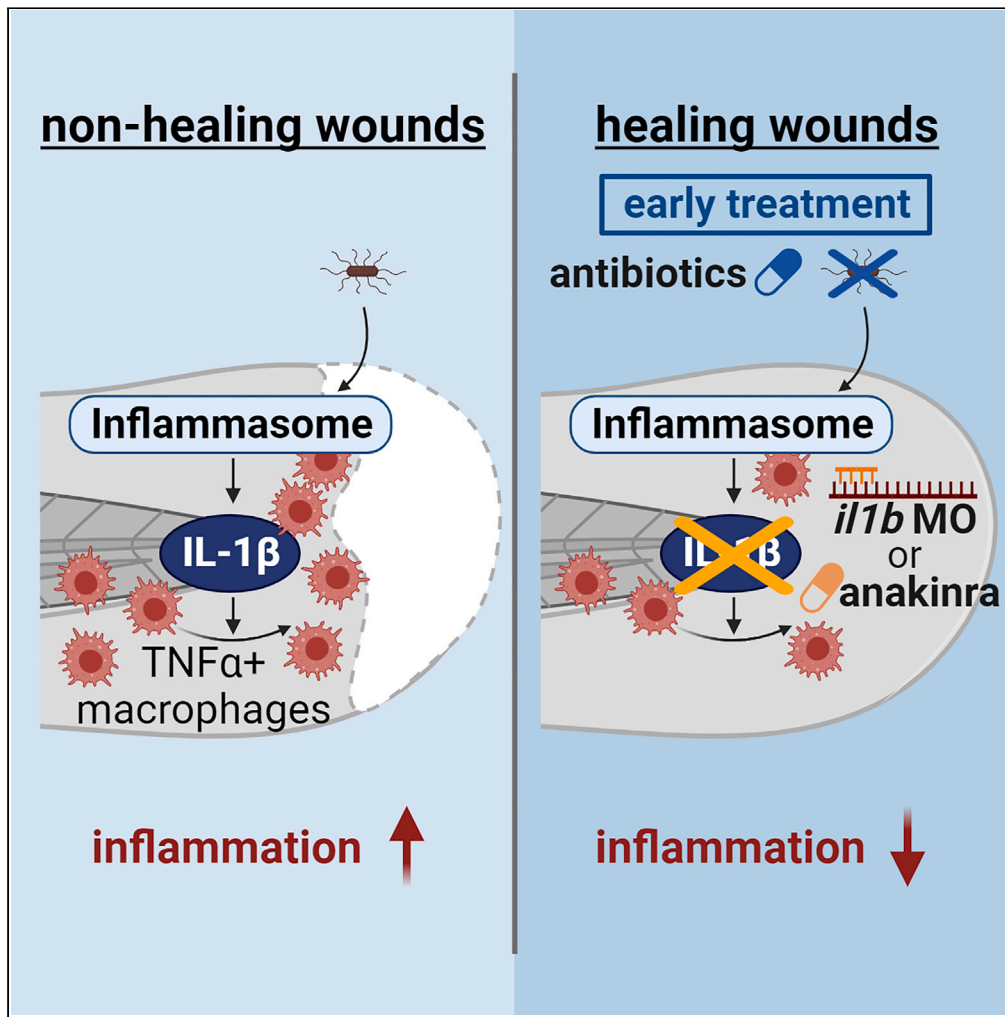


Article

Infection induced inflammation impairs wound healing through IL-1 β signaling



Simone Shen,
Veronika Miskolci,
Colin N. Dewey,
John-Demian
Sauer, Anna
Huttenlocher

sauer3@wisc.edu (J.-D.S.)
huttenlocher@wisc.edu (A.H.)

Highlights

Bacteria induced
inflammation impairs
wound healing

Blocking IL-1 β signaling
improves wound healing in
bacterial-infected wounds

Early eradication of
bacteria resolves
inflammation at the wound

Inflammation resolution
correlates with improved
wound healing after
infection

Shen et al., iScience 27, 109532
April 19, 2024 © 2024 The
Author(s). Published by Elsevier
Inc.
[https://doi.org/10.1016/
j.isci.2024.109532](https://doi.org/10.1016/j.isci.2024.109532)

Article

Infection induced inflammation impairs wound healing through IL-1 β signalingSimone Shen,¹ Veronika Miskolci,^{1,4} Colin N. Dewey,² John-Demian Sauer,^{1,*} and Anna Huttenlocher^{1,3,5,*}

SUMMARY

Wound healing is impaired by infection; however, how microbe-induced inflammation modulates tissue repair remains unclear. We took advantage of the optical transparency of zebrafish and a genetically tractable microbe, *Listeria monocytogenes*, to probe the role of infection and inflammation in wound healing. Infection with bacteria engineered to activate the inflammasome, Lm-Pyro, induced persistent inflammation and impaired healing despite low bacterial burden. Inflammatory infections induced *il1b* expression and blocking IL-1R signaling partially rescued wound healing in the presence of persistent infection. We found a critical window of microbial clearance necessary to limit persistent inflammation and enable efficient wound repair. Taken together, our findings suggest that the dynamics of microbe-induced tissue inflammation impacts repair in complex tissue damage independent of bacterial load, with a critical early window for efficient tissue repair.

INTRODUCTION

Microbial infection is a common complication and leading cause of chronic non-healing wounds.^{1,2} Inflammatory responses are critical for pathogen detection and clearance, but when excessive or prolonged can also interfere with wound healing.^{3,4} However, how immune responses triggered by microbes can impair wound healing remains unclear.

Caudal fin transection of larval zebrafish provides a powerful *in vivo* model to understand immune responses during infection and wound repair. When larval zebrafish transected wounds are infected with *Listeria monocytogenes* (*Lm*), there is an increase in neutrophil and macrophage infiltration at wounds compared to a sterile wound, and wound healing is impaired.³ In contrast, when transected wounds are infected with a Δhly mutant, a *Lm* mutant unable to escape from the phagosome to the host cytosol due to loss of the gene encoding listeriolysin-O (LLO),⁵ there is no defect in wound healing.³ Infection by Δhly mutants is also associated with less inflammation and bacterial load at the wound site compared to wild-type (WT) *Lm* infection.³ This led us to hypothesize that infection-induced inflammation may drive the defect in wound healing in this model.

Lm stimulates inflammation through multiple pattern recognition receptors (PRRs), including toll-like receptor (TLR),⁶ stimulator of interferon genes (STING),⁷ and nucleotide oligomerization domain (NOD)-like receptors (NLRs).^{8–10} Multiple NLRs, including NLRP3^{9,10} and NLRC4¹¹ are induced by *Lm*. These NLRs, as well as AIM2 triggered by *Lm* DNA, form inflammasome complexes that activate caspase-1.^{12–14} Caspase-1 activation subsequently cleaves and activates IL-1 β . A previous study from our group showed that Lm-Pyro, a *Lm* strain engineered to hyperactivate the inflammasome triggers robust inflammation and is attenuated in zebrafish.¹⁵

In this study, we demonstrate that inflammation associated with infection impairs wound healing of larval zebrafish. When transection wounds were infected with Lm-Pyro that triggers extensive inflammation through hyperactivation of the inflammasome, wound healing was impaired although there was attenuation in bacteria virulence. Furthermore, RNA-seq identified an inflammatory profile, with increased expression of *il1b*. We utilized genetic and pharmacological approaches to demonstrate that IL-1 β stimulated by *Lm* infection inhibits wound healing. Finally, we found that early eradication of infection is critical to prevent non-resolving inflammation and impaired wound healing. Taken together, our data establish that persistent inflammation associated with bacterial infection inhibits wound healing and that the use of clinically approved IL-1R antagonists, or early antibiotic intervention, can improve healing outcomes of infected wounds in zebrafish larvae.

RESULTS

***L. monocytogenes* that hyperactivates the inflammasome impairs wound healing despite rapid clearance**

Microbes stimulate inflammation through multiple PRRs including TLRs and NLRs that lead to activation of different innate immune signaling pathways.^{6,16,17} We previously demonstrated that Δhly *Lm* mutant that fails to escape the phagosome into the host cell cytosol and has attenuated

¹Department of Medical Microbiology and Immunology, University of Wisconsin-Madison, Madison, WI, USA

²Department of Biostatistics and Medical Informatics, University of Wisconsin-Madison, Madison, WI, USA

³Department of Pediatrics, University of Wisconsin-Madison, Madison, WI, USA

⁴Present address: Department of Microbiology, Biochemistry and Molecular Genetics, Center for Cell Signaling, Center for Immunity and Inflammation, Rutgers New Jersey Medical School, Newark, NJ, USA

⁵Lead contact

*Correspondence: sauer3@wisc.edu (J.-D.S.), huttenlocher@wisc.edu (A.H.)

<https://doi.org/10.1016/j.isci.2024.109532>



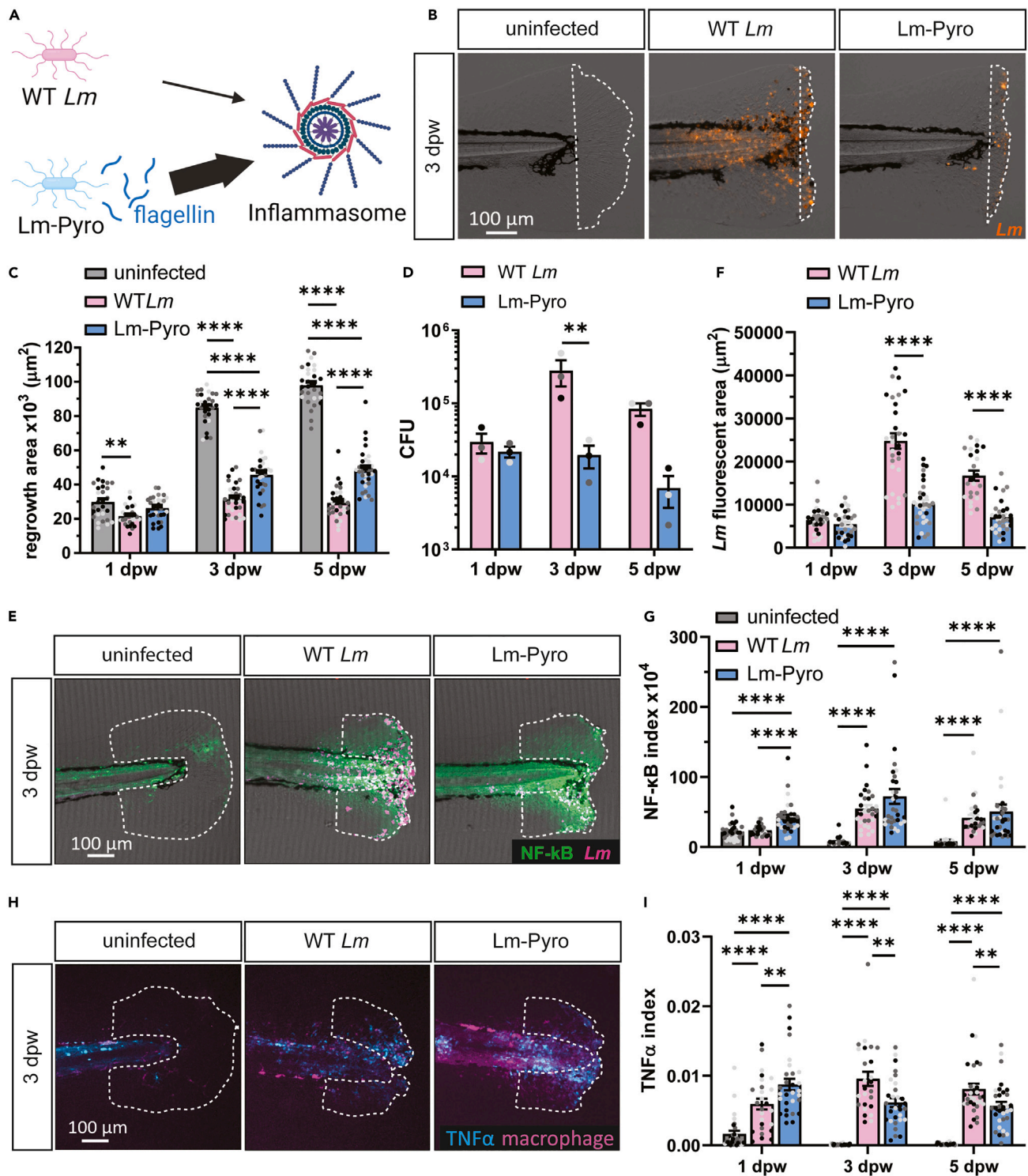


Figure 1. Inflammation stimulated by inflammasome signaling impairs wound healing in *Lm*-infected zebrafish larvae

(A) *Lm*-Pyro hyperactivates the inflammasome through secretion of flagellin.

(B) Representative merged images of single-plane brightfield and fluorescent images of the caudal fin of zebrafish larvae in response to WT *Lm* or *Lm*-Pyro infection over time using mCherry-expressing *Lm*, and the corresponding quantification of tissue regrowth from three biological replicates are shown in (C). White dashed line in (B) outlines regrowth area. N = 28–32 larvae per treatment per time point.

(D) CFU of *Lm* was determined at indicated timepoints by pooling 10 zebrafish larvae per condition per time point.

Figure 1. Continued

(E) Representative sum-projections of z stacks of the caudal fin acquired by laser scanning confocal microscope using *Tg(NF-κB:EGFP)* larvae and mCherry-expressing *Lm* fixed at indicated time points. NF-κB is shown in green and *Lm* is shown in magenta. White dashed line denotes the wound sites, where NF-κB was quantified. The corresponding quantification of *Lm* fluorescent area at the tail fins quantified by area thresholding is shown in (F) and NF-κB index showing NF-κB integrated intensity normalized to regrowth area is plotted in (G).

(E–G) N = 24–33 larvae per treatment per time point.

(H) Representative sum-projections of z stacks acquired by laser scanning confocal microscope using double transgenic larvae (*Tg(tnfa:GFP)* × *Tg(mpeg1:mCherry-CAAX)*) over time in response to uninfected, WT *Lm*-infected, or *Lm*-Pyro-infected wounds. TNFα is shown in cyan and macrophages are shown in magenta. White dashed line denotes area measured for TNFα+ macrophages area. Corresponding quantification is plotted in (I) with TNFα index showing percentage of TNFα positive macrophages quantified by area thresholding and normalized by regrowth fin area.

(H and I) N = 25–32 larvae per treatment per time point. Values in (C), (D), (F), (G), and (I) are arithmetic means and SE with associated p values obtained by least square mean analysis in (C), two-way ANOVA in (D), and rank analysis due to residuals not being normally distributed in (F), (G), and (I). Three biological replicates were performed with data points from different biological replicates displayed in different shades of gray. *p < 0.05, **p < 0.01, ***p < 0.001, ****p < 0.0001. See also [Figure S1](#).

virulence,⁵ does not inhibit wound healing in zebrafish larvae.³ This led to the hypothesis that the cytosolic innate immune signaling activated by *Lm* may impair wound healing. An important inflammatory response dependent on *Lm* access to the cytosol is activation of the inflammasome.^{9,10,12–14} To address how inflammasome activation may affect wound healing, we took advantage of a *Lm* mutant, *Lm*-Pyro, that hyperactivates the inflammasome via ectopic secretion of flagellin but also has reduced virulence ([Figure 1A](#)).^{11,15,18} In accordance with prior reports, *Lm*-Pyro was attenuated in the zebrafish wound model with decreased bacterial burden compared to WT *Lm* infection ([Figure 1D](#)).¹⁵ Early on during infection, WT *Lm* and *Lm*-Pyro started off at similar burden at 1 day-post-wound (dpw). Over time, at 3 dpw, we observed significantly reduced bacterial burden in *Lm*-Pyro-infected compared to WT *Lm*-infected larvae, indicating attenuation in virulence as expected. At 5 dpw, we saw a similar trend, but the difference was not statistically significant ([Figure 1D](#)). Although wound healing was slightly improved compared to WT *Lm*-infected larvae, it was still severely impaired in *Lm*-Pyro-infected compared to uninfected larvae despite *Lm*-Pyro having a lower bacterial burden ([Figures 1B](#) and [1C](#)). To determine if hyperactivation of the inflammasome, despite the attenuation in *Lm*-Pyro infection, still triggers hyperinflammation at the wound site, we quantified NF-κB expression at the wound microenvironment using *Tg(NF-κB:EGFP)* zebrafish.¹⁹ In this study, we define the wound microenvironment or wound site as the caudal fin tissue area distal to the caudal vein loop excluding the notochord.³ To visualize spread of infection, we utilized WT *Lm* and *Lm*-Pyro expressing red fluorescent protein, mCherry. We found at 3 and 5 dpw, there was less burden of *Lm*-Pyro compared to WT *Lm* at the tail fins, as suggested by the smaller mCherry fluorescent area, which is consistent with the results obtained by CFU plating ([Figures 1D](#) and [1F](#)). At early stage infection, 1 dpw, there was a higher level of NF-κB at the wound site in *Lm*-Pyro-infected wounds compared to WT *Lm*-infected and uninfected wounds, suggesting *Lm*-Pyro triggered hyperinflammation early after infection. At 3 and 5 dpw, when there was a lower burden of *Lm*-Pyro at the infected tail wounds, both WT *Lm* and *Lm*-Pyro highly induced NF-κB at the wound site, suggesting that both types of infections stimulated extensive and prolonged inflammation independent of bacterial load ([Figures 1E](#) and [1G](#)). We have previously shown that *Lm* infection increases recruitment of pro-inflammatory macrophages to the wound site.³ To further assess if hyperactivation of the inflammasome affects the inflammatory state of the macrophages at the wound, pro-inflammatory wound-associated macrophages were identified using a transgenic reporter line for TNFα expression crossed to a line that labels all macrophages (*Tg(tnfa:GFP)* × *Tg(mpeg1.1:mCherry-CAAX)*).^{3,20–22} We found that more macrophages were recruited to the wound sites in WT *Lm*-infected and *Lm*-Pyro-infected wounds at 1, 3, and 5 dpw compared to uninfected wounds ([Figure S1A](#)). The macrophages at the wound site in WT *Lm*-infected and *Lm*-Pyro-infected wounds both persistently expressed TNFα, indicating that both WT *Lm* and *Lm*-Pyro triggered hyperinflammation early and the inflammation was persistent even after the bacteria started to clear ([Figures 1H](#), [1I](#), and [S1B](#)). These findings suggest that extensive inflammation stimulated by infection, and particularly inflammasome activation, can impair wound healing independent of bacterial burden.

***L. monocytogenes* upregulates *il1b* at zebrafish tail wounds**

Our findings suggest that *Lm*-stimulated inflammation correlates with impaired wound healing. We therefore hypothesized that a specific signature of inflammation may be associated with infected wounds. To identify the signature, we performed bulk RNA sequencing on uninfected, WT *Lm*-infected, or *Lm*-Pyro-infected tail wounds. We identified *il1b* as one of the top upregulated genes in both WT *Lm* infection and *Lm*-Pyro infection ([Figures 2A](#), [2B](#), and [2E](#); [Data S1](#)). Indeed, the change in gene signature induced by WT *Lm* and *Lm*-Pyro were surprisingly similar ([Figure 2C](#)). We found that there were 22 genes that were upregulated more than 2-fold in WT *Lm*-infected tail wounds compared to uninfected tail wounds, and all 22 genes were also upregulated more than 2-fold with *Lm*-Pyro infection ([Figure 2D](#)). Among the 22 genes that were induced by both WT *Lm* and *Lm*-Pyro infections, *il1b* was the fifth most upregulated gene ([Figures 2D](#) and [2E](#); [Table S1](#)). Other top candidates were less well characterized in zebrafish and included *acod1* and chemokine ligand 35. To validate RNA-sequencing results, we focused on *il1b* and confirmed the upregulation of *il1b* expression in zebrafish tail wounds infected with both WT *Lm* and *Lm*-Pyro infections compared to uninfected wounds ([Figure 2F](#)). In contrast, *Δhly*, which does not induce hyperinflammation or affect wound healing,³ had no effect on *il1b* expression of infected tail wounds ([Figure 2F](#)). These findings suggest that increased IL-1β induced by infection may be detrimental to wound healing.

***L. monocytogenes* infection inhibits wound healing through IL-1β signaling**

To test the hypothesis that *Lm*-induced *il1b* expression impairs wound healing, we tested the effects of inhibition of IL-1β using both genetic and pharmacological approaches. *il1b* was depleted using an antisense morpholino oligonucleotide (MO)²³ that was confirmed by changes in

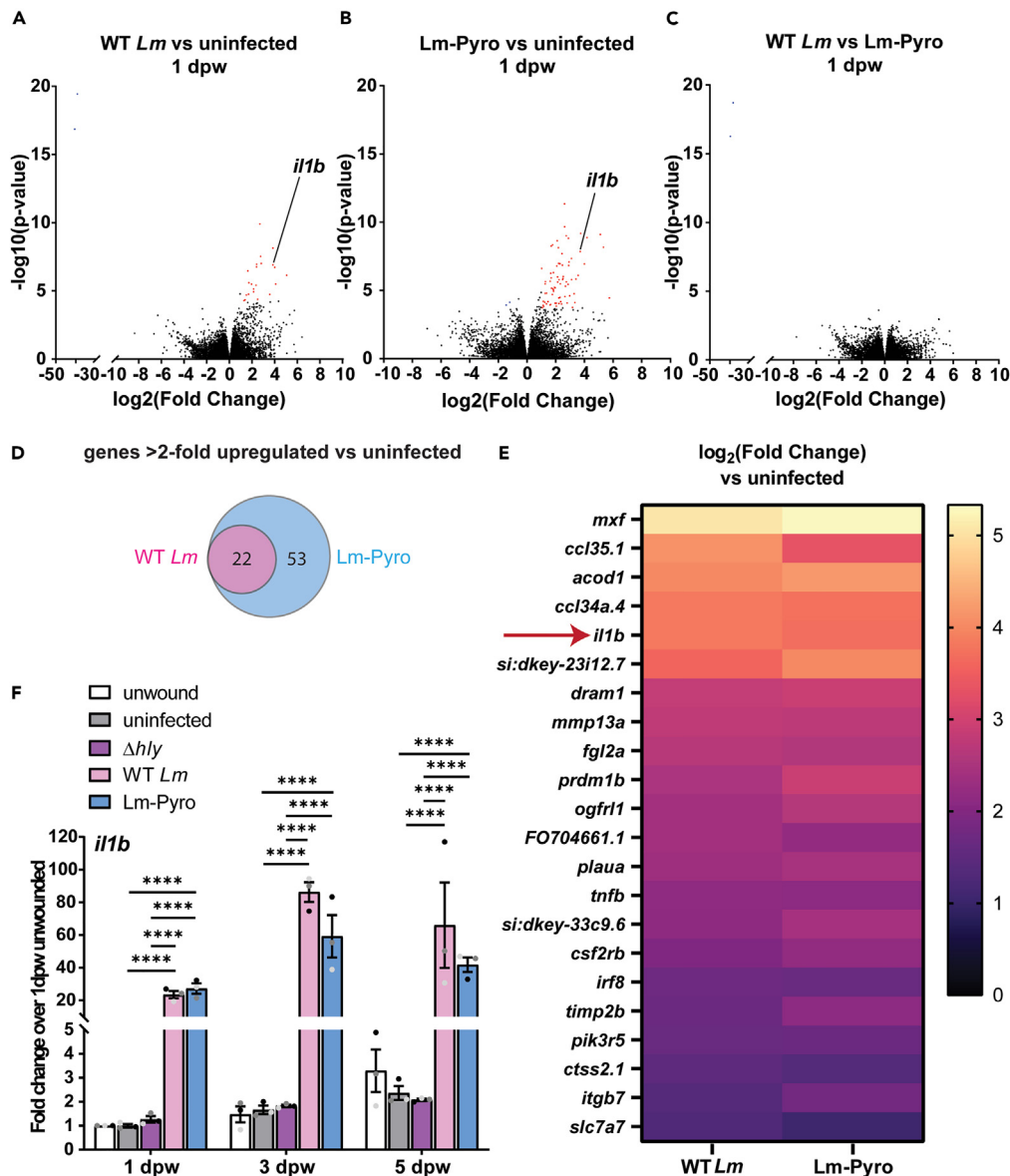


Figure 2. Transcriptomic analysis identifies *il1b* as an inflammatory marker in *Lm*-infected wounds

(A) Volcano plot for gene expression comparison between (A) uninfected and WT *Lm*-infected, (B) uninfected and Lm-Pyro infected, and (C) WT *Lm*-infected and Lm-Pyro-infected tail fins at 1 dpw obtained by RNA sequencing. (A–C) Red dots depict more than 2-fold upregulated genes and blue dots depict more than 2-fold downregulated genes for with Benjamini-Hochberg corrected p value < 0.05 for each comparison.

(D) Venn diagram depicting genes that are more than 2-fold upregulated compared to uninfected condition in WT *Lm*-infected and Lm-Pyro-infected tail wounds, with the overlapping gene lists shown in a heatmap in (E). (A–E) n = 50 per treatment per biological replicate with three biological replicates.

(F) *il1b* expression normalized to fold change over 1 dpw uninfected condition in pooled tail fin tissue collected from larvae from each treatment at indicated time points measured by RT-qPCR from three biological replicates with n = 18–25 larvae per treatment per time point per biological replicate. (F) is showing arithmetic means and SE with associated p values obtained by two-way ANOVA performed on RT-qPCR ΔC_q values. Data points from different biological replicates are displayed in different shades of gray. ****p < 0.0001. See Table S1 for detailed information on upregulated genes shown in (E).

il1b mRNA splicing (Figure 3B). To determine if knocking down *il1b* affects bacterial clearance in the zebrafish, mCherry-expressing *Lm* were used, and we found no difference in bacterial burden between standard control MO (std MO) and *il1b* MO injections in either WT *Lm*-infected or Lm-Pyro-infected larvae (Figure 3C). In both WT *Lm*-infected and Lm-Pyro-infected zebrafish, when *il1b* was knocked down, there was improved wound healing compared to std MO injected larvae (Figure 3D). There was also reduced inflammation in the IL-1 β -deficient larvae, as suggested by the decreased NF- κ B expression upon depletion of *il1b* (Figure 3E). To complement gene depletion, we took a pharmacological approach to inhibit IL-1 β signaling using anakinra, an antagonist of interleukin-1 receptor (IL-1Ra). Blocking IL-1 signaling with anakinra

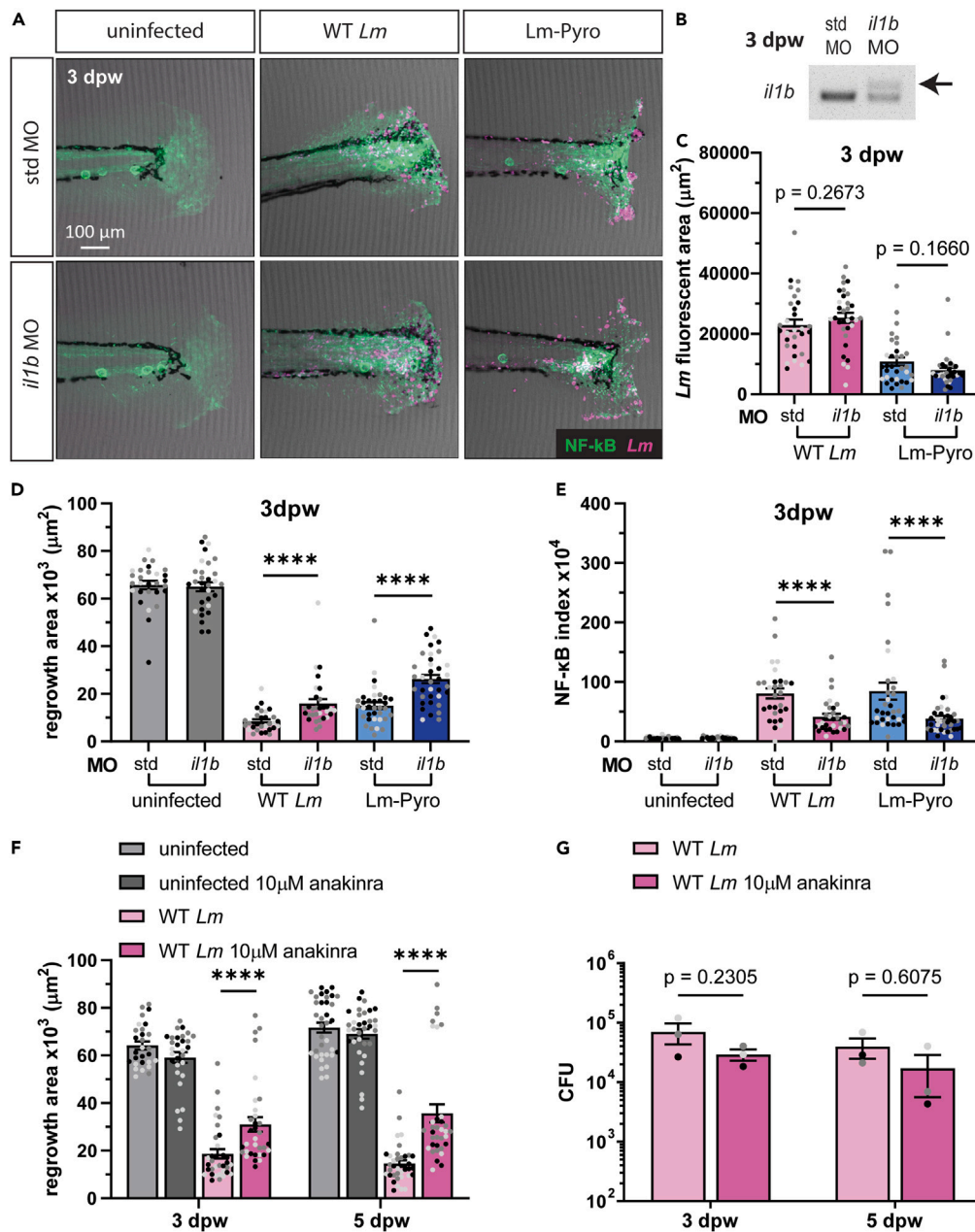


Figure 3. *Lm* inhibits wound healing through IL-1 β signaling

(A) Representative images for sum-projections of z stacks acquired by laser scanning confocal microscope using std MO- or *il1b* MO-injected *Tg(NF- κ B:EGFP)* zebrafish larvae and mCherry-expressing *Lm* fixed at 3 dpw. NF- κ B signal is shown in green and *Lm* shown in magenta. Scale bar is 100 microns.

(B) PCR amplification of *il1b* cDNA from std MO- or *il1b* MO-injected larvae at 3 dpw. Quantification of (C) *Lm* fluorescent area at the tail fins using area thresholding, (D) regrowth area of the tail fins and (E) integrated intensity for background-corrected NF- κ B normalized to regrowth area shown as NF- κ B index from images in (A) from three biological replicates with $n = 28$ –36.

(F and G) 1 day-post-fertilization larvae were treated with 10 μ M anakinra with quantification of regrowth area over time in (F). (G) CFU of *Lm* was determined at indicated timepoints by pooling 10 larvae per condition per time point from three biological replicates. (F) Regrowth area was quantified from three biological replicates with $N = 28$ –36 larvae per treatment per time point. (C–G) are arithmetic means and SE with associated p values obtained by least square mean analysis in (C), rank analysis due to residuals not being normally distributed in (D–F), and two-way ANOVA in (G). Data points from different biological replicates are displayed in different shades of gray. * $p < 0.05$, ** $p < 0.01$, *** $p < 0.001$, **** $p < 0.0001$. See also Figure S2.

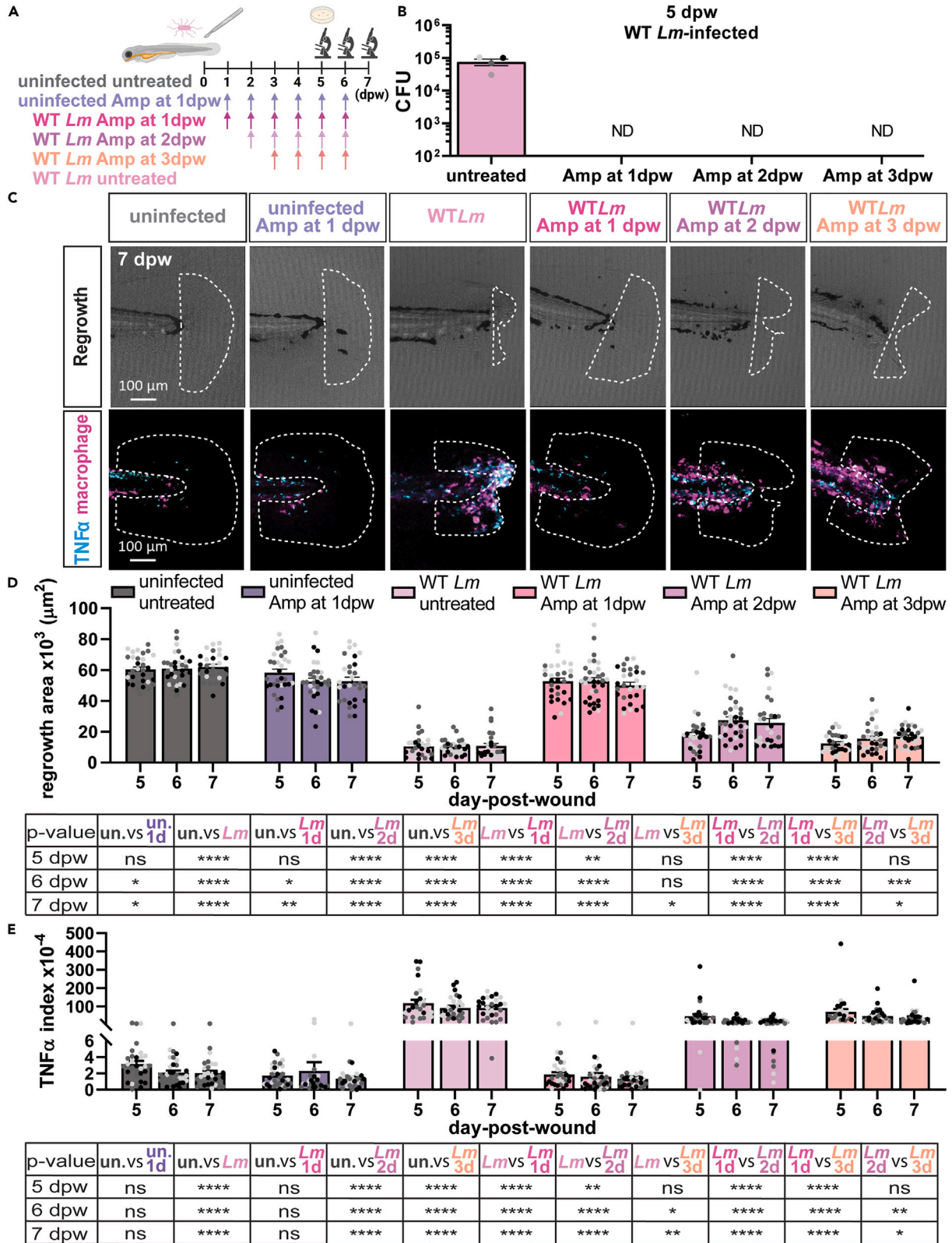


Figure 4. Early eradication of *Lm* infection is required for inflammation resolution and wound healing

(A) Experimental setup is shown. Double transgenic WT larvae (*Tg(tnfa:GFP) x Tg(mpeg1:mCherry-CAAX)*) fixed and imaged at indicated timepoints (5–7 dpw) following uninfected, WT *Lm*-infected, or WT *Lm*-infected tail transection at 3 dpf that were treated with ampicillin starting at 1, 2, or 3 dpw. (B) CFU of *Lm* at 5 dpw was determined by pooling 10 zebrafish larvae per condition per time point from four biological replicates. (C) Representative sum-projections of z stack images at 7 dpw acquired by laser scanning confocal microscope are shown. Tail wounds were also imaged at 5 and 6 dpw, but only the 7 dpw time point is shown. White dashed line on top row outlines regrowth area and on bottom row denotes area for TNF α + macrophage quantification. TNF α is shown in cyan and macrophages are shown in magenta. Scale bar is 100 microns. (D) Corresponding quantification of regrowth area of larvae at 5, 6, and 7 dpw using dataset in (C), and in (E) corresponding quantification of TNF α index showing TNF α + macrophages were quantified by area thresholding and normalized to regrowth area. (C–E) from three biological replicates with total N = 27–34 larvae per treatment per time point. (B), (D), and (E) are arithmetic means and SE with associated p values obtained by two-way ANOVA in (B) and rank analysis in (D) and (E). Data points from different biological replicates are displayed in different shades of gray. **p < 0.01, ****p < 0.0001. Amp, ampicillin; un., uninfected; un. 1 day, uninfected Amp at 1 dpw; *Lm* 1 day, *Lm*-infected Amp at 1 dpw; *Lm* 2 days, *Lm*-infected Amp at 2 dpw; *Lm* 3 days, *Lm*-infected Amp at 3 dpw.

did not affect wound healing in uninfected zebrafish; however, it improved wound healing in *Lm*-infected tail wounds (Figure 3F). Anakinra treatment also dampened inflammation at the wound site in *Lm*-infected wounds as suggested by the decreased abundance of pro-inflammatory (TNF α +) macrophages at the tail wounds (Figure S2). Importantly, anakinra was able to improve wound healing without affecting bacterial clearance (Figure 3G). Taken together, these findings suggest that *Lm*-induced inflammation impairs wound healing, at least in part, via IL-1 β signaling.

Early clearance of *L. monocytogenes* is necessary to prevent persistent inflammation and enable wound healing

To determine if clearance of bacteria would resolve inflammation and restore wound healing, we tested the effects of antibiotic treatment with ampicillin. In addition, to investigate if the timing of antibiotics administration is critical, we treated *Lm*-infected larvae with ampicillin starting at 1, 2, or 3 dpw (Figure 4A). Under all conditions, ampicillin treatment effectively cleared infection completely by 5 dpw (Figure 4B). Surprisingly, only early treatment with ampicillin starting at 1 dpw rescued wound healing by 5 dpw (Figure 4D). Even at 6 and 7 dpw, *Lm*-infected larvae treated with ampicillin at a later time point, at either 2 or 3 dpw, still displayed impaired wound healing (Figures 4C and 4D). To assess if inflammation is altered by ampicillin treatment, pro-inflammatory (TNF α +) macrophages at the wound sites were quantified. Ampicillin treatment starting at any stage of infection reduced TNF α -expressing macrophages; however, only treatment starting at 1 dpw dampened inflammation to uninfected levels (Figures 4C and 4E). This provides further support for the idea that resolution of inflammation at the wound site correlates with improved wound healing in the early ampicillin treatment group. At 6 and 7 dpw, later treatment with ampicillin still did not resolve the presence of TNF α -expressing macrophages at the wound site, indicating non-resolving inflammation (Figures 4C and 4E). Our findings suggest that there is a critical window for bacterial clearance necessary to limit prolonged inflammation and promote tissue repair.

DISCUSSION

Bacterial infection has long been associated with defects in wound healing, however the mechanisms remain unclear.⁴ In humans, wound healing involves four distinct phases: hemostasis, inflammation, proliferation, and resolution.²⁴ Zebrafish larvae share similar wound healing characteristics although lack the blood-clotting step during the initial hemostasis phase.²⁵ Accordingly, re-epithelization is an early wound healing phase in larval zebrafish and in general, zebrafish tissue regenerates after inflammation resolves.²⁵

Taking advantage of this simplified wound healing model in zebrafish larvae, here we show that infection-induced inflammation impairs wound healing independent of bacterial burden. We demonstrate that non-resolving inflammation triggered by infection leads to dysregulation of the inflammation phase of wound healing resulting in impaired tissue repair. We provide evidence that there is a critical window during which bacterial clearance can abrogate chronic tissue inflammation. Interestingly, clearance of infection after this critical window is not sufficient to improve tissue repair. However, resolving inflammation by knocking down *il1b* or by blocking IL-1 signaling with anakinra, an IL-1R antagonist, was able to partly rescue the defect in wound healing even in the presence of persistent bacterial burden. Taken together, our findings suggest that persistent inflammation induced by infection is sufficient to limit tissue repair even after the infection is cleared.

Our gene expression analysis demonstrated that *il1b* expression was induced by both WT *Lm* and *Lm*-Pyro. Our findings suggest that *il1b* expression is a common signature of infected and inflammatory non-healing wounds, independent of bacterial load. In diabetic fibroblast *ex vivo* models, high levels of IL-1 β inhibit cell proliferation.²⁶ Additionally, in diabetic mice, treatment with IL-1 β -neutralizing antibody shifted the macrophage phenotype from a pro-inflammatory state to a pro-healing state and improved wound healing.²⁷ Infected wounds share similar characteristics as diabetic chronic wounds where both types of non-healing wounds often exhibit polymicrobial infections and prolonged inflammatory responses.²⁸ In this study, we demonstrated that IL-1 β signaling triggered by infection inhibits wound healing and that IL-1R blockade with anakinra improved wound healing in *Lm*-infected zebrafish tail wounds. Importantly, anakinra treatment did not affect bacterial burden. This suggests that IL-1 β could serve as a potential therapeutic target for treating infected wounds.

Additionally, our RNA-seq analysis suggested that there were other inflammatory profiles that were highly upregulated by infections, such as immune-responsive gene 1 (*irg1*), also known as aconitate decarboxylase (*acod1*), which could potentially serve as an alternative target for dampening inflammation during wound healing. However, inhibiting inflammation in the setting of infection can pose a significant challenge since inflammation plays an essential role in host defense against infections. Studies have shown *irg1* to be essential for clearance of *Mycobacterium tuberculosis* (*Mtb*) infection.²⁹ In contrast, there is attenuation in *S. aureus* virulence in *irg1*-deficient mice.³⁰ Future studies are

needed to further examine the role of *irg1* in wound healing and host defense against infection to determine if *irg1* could be a potential target for treating infected wounds. It is critical to identify inflammatory targets that do not link to host defense.

Treatment of infected wounds typically involves the use of antimicrobial agents to reduce bacterial colonization at the wound and promote wound healing.^{31–33} Indeed, current treatments for infected wounds focus on killing the bacteria with antibiotics.^{34,35} Our findings suggest that post-infection, there is a narrow therapeutic window for antibiotic treatment before chronic inflammation is established. It will be interesting to determine if a similar critical window is also true for humans with infected wounds. Overall, our findings suggest that future therapeutics for infected wounds, including surgical site infections, could combine antibiotic treatment with anti-inflammatory agents that limit inflammation triggered by infections to further facilitate wound healing.

In conclusion, our data demonstrate that sustained inflammation induced by infection limits tissue repair in zebrafish larvae. This study supports our prior work which showed a correlation between the presence of inflammatory macrophages (TNF α positive) and impaired wound healing.³⁶ Here, we show that inflammasome activation and induction of *il1b* is associated with impaired wound healing independent of bacterial burden. Early events during infection induced inflammation appear to influence long-term healing outcome, since only early antibiotics treatment facilitated repair. This work raises the interesting question about the combined use of antibiotics and anti-inflammatory agents such as an IL-1 receptor antagonist to treat infected wounds.

Limitations of the study

However, one limitation in our experimental setup was that the absolute bacterial burden at different time points pre-ampicillin treatment was different; therefore, we cannot rule out that the extent of infection was not driving the differences observed in wound healing between zebrafish larvae treated with ampicillin at varying time points. In addition, the application of these findings to human wounds remains unknown.

STAR★METHODS

Detailed methods are provided in the online version of this paper and include the following:

- KEY RESOURCES TABLE
- RESOURCE AVAILABILITY
 - Lead contact
 - Materials availability
 - Data and code availability
- EXPERIMENTAL MODEL AND STUDY PARTICIPANT DETAILS
 - Zebrafish Husbandry and Handling
 - Bacterial strains
- METHOD DETAILS
 - Zebrafish wounding and infection
 - Fixation
 - Tissue regrowth area measurement
 - NF- κ B quantification
 - Macrophage and TNF α expression quantification
 - Bacterial burden quantification
 - RNA sequencing
 - RNA sequencing analysis
 - RT-qPCR
 - Morpholino injections
 - Drug treatment
- QUANTIFICATION AND STATISTICAL ANALYSIS

SUPPLEMENTAL INFORMATION

Supplemental information can be found online at <https://doi.org/10.1016/j.isci.2024.109532>.

ACKNOWLEDGMENTS

We thank Dr. Warren Rose at University of Wisconsin-Madison School of Pharmacy for access to anakinra. This work was supported by NIH GM118027 (A.H.), NIH 1R01AI137070 and NIH 1R21AI173738 (J.D.S.), and NIH K99GM138699 and AHA 17POST33410970 (V.M.). Figure diagrams and graphical abstract were made with biorender.com.

AUTHOR CONTRIBUTIONS

Conceptualization, S.S., J.D.S., and A.H.; formal analysis, S.S., V.M., and C.N.D.; methodology, S.S., J.D.S., and A.H.; investigation, S.S.; visualization, S.S.; writing – original draft, S.S.; writing – review and editing, S.S., V.M., C.N.D., J.D.S., and A.H.; funding acquisition, V.M., J.D.S., and A.H.

DECLARATION OF INTERESTS

The authors declare no competing interests.

Received: July 11, 2023

Revised: January 14, 2024

Accepted: March 16, 2024

Published: March 19, 2024

REFERENCES

1. Leaper, D., Assadian, O., and Edmiston, C.E. (2015). Approach to chronic wound infections. *Br. J. Dermatol.* 173, 351–358. <https://doi.org/10.1111/bjd.13677>.
2. Bessa, L.J., Fazio, P., Di Giulio, M., and Cellini, L. (2015). Bacterial isolates from infected wounds and their antibiotic susceptibility pattern: some remarks about wound infection. *Int. Wound J.* 12, 47–52. <https://doi.org/10.1111/iwj.12049>.
3. Miskolci, V., Squirrell, J., Rindy, J., Vincent, W., Sauer, J.D., Gibson, A., Eliceiri, K.W., and Huttenlocher, A. (2019). Distinct inflammatory and wound healing responses to complex caudal fin injuries of larval zebrafish. *Elife* 8, e45976. <https://doi.org/10.7554/eLife.45976>.
4. Zhao, R., Liang, H., Clarke, E., Jackson, C., and Xue, M. (2016). Inflammation in Chronic Wounds. *Int. J. Mol. Sci.* 17, 2085. <https://doi.org/10.3390/ijms17122085>.
5. Jones, S., and Portnoy, D.A. (1994). Characterization of *Listeria monocytogenes* pathogenesis in a strain expressing perfringolysin O in place of listeriolysin O. *Infect. Immun.* 62, 5608–5613. <https://doi.org/10.1128/iai.62.12.5608-5613.1994>.
6. Flo, T.H., Halaas, O., Lien, E., Ryan, L., Teti, G., Golenbock, D.T., Sundan, A., and Espevik, T. (2000). Human toll-like receptor 2 mediates monocyte activation by *Listeria monocytogenes*, but not by group B streptococci or lipopolysaccharide. *J. Immunol.* 164, 2064–2069. <https://doi.org/10.4049/jimmunol.164.4.2064>.
7. Woodward, J.J., Iavarone, A.T., and Portnoy, D.A. (2010). c-di-AMP secreted by intracellular *Listeria monocytogenes* activates a host type I interferon response. *Science* 328, 1703–1705. <https://doi.org/10.1126/science.1189801>.
8. Özören, N., Masumoto, J., Franchi, L., Kanneganti, T.D., Body-Malapel, M., Ertürk, I., Jagirdar, R., Zhu, L., Inohara, N., Bertin, J., et al. (2006). Distinct roles of TLR2 and the adaptor ASC in IL-1 β /IL-18 secretion in response to *Listeria monocytogenes*. *J. Immunol.* 176, 4337–4342. <https://doi.org/10.4049/jimmunol.176.7.4337>.
9. Mariathasan, S., Weiss, D.S., Newton, K., McBride, J., O'Rourke, K., Roose-Girma, M., Lee, W.P., Weinrauch, Y., Monack, D.M., and Dixit, V.M. (2006). Cryopyrin activates the inflammasome in response to toxins and ATP. *Nature* 440, 228–232. <https://doi.org/10.1038/nature04515>.
10. Meixenberger, K., Pache, F., Eitel, J., Schmeck, B., Hippenstiel, S., Slevogt, H., N'Guessan, P., Witznath, M., Netea, M.G., Chakraborty, T., et al. (2010). *Listeria monocytogenes*-infected human peripheral blood mononuclear cells produce IL-1 β , depending on listeriolysin O and NLRP3. *J. Immunol.* 184, 922–930. <https://doi.org/10.4049/jimmunol.0901346>.
11. Sauer, J.D., Pereyre, S., Archer, K.A., Burke, T.P., Hanson, B., Lauer, P., and Portnoy, D.A. (2011). *Listeria monocytogenes* engineered to activate the Nlr4 inflammasome are severely attenuated and are poor inducers of protective immunity. *Proc. Natl. Acad. Sci. USA* 108, 12419–12424. <https://doi.org/10.1073/pnas.1019041108>.
12. Sauer, J.D., Witte, C.E., Zemansky, J., Hanson, B., Lauer, P., and Portnoy, D.A. (2010). *Listeria monocytogenes* triggers AIM2-mediated pyroptosis upon infrequent bacteriolysis in the macrophage cytosol. *Cell Host Microbe* 7, 412–419. <https://doi.org/10.1016/j.chom.2010.04.004>.
13. Warren, S.E., Mao, D.P., Rodriguez, A.E., Miao, E.A., and Aderem, A. (2008). Multiple Nod-like receptors activate caspase 1 during *Listeria monocytogenes* infection. *J. Immunol.* 180, 7558–7564. <https://doi.org/10.4049/jimmunol.180.11.7558>.
14. Wu, J., Fernandes-Alnemri, T., and Alnemri, E.S. (2010). Involvement of the AIM2, NLRC4, and NLRP3 inflammasomes in caspase-1 activation by *Listeria monocytogenes*. *J. Clin. Immunol.* 30, 693–702. <https://doi.org/10.1007/s10875-010-9425-2>.
15. Vincent, W.J.B., Freisinger, C.M., Lam, P.Y., Huttenlocher, A., and Sauer, J.D. (2016). Macrophages mediate flagellin induced inflammasome activation and host defense in zebrafish. *Cell Microbiol.* 18, 591–604. <https://doi.org/10.1111/cmi.12536>.
16. Takeuchi, O., and Akira, S. (2010). Pattern recognition receptors and inflammation. *Cell* 140, 805–820. <https://doi.org/10.1016/j.cell.2010.01.022>.
17. Opitz, B., Eitel, J., Meixenberger, K., and Suttrop, N. (2009). Role of Toll-like receptors, NOD-like receptors and RIG-I-like receptors in endothelial cells and systemic infections. *Thromb. Haemost.* 102, 1103–1109. <https://doi.org/10.1160/TH09-05-0323>.
18. Theisen, E., and Sauer, J.D. (2017). *Listeria monocytogenes*-Induced Cell Death Inhibits the Generation of Cell-Mediated Immunity. *Infect. Immun.* 85, e07333-16. <https://doi.org/10.1128/IAI.00733-16>.
19. Kanther, M., Sun, X., Mühlbauer, M., Mackey, L.C., Flynn, E.J., 3rd, Bagnat, M., Jobin, C., and Rawls, J.F. (2011). Microbial colonization induces dynamic temporal and spatial patterns of NF- κ B activation in the zebrafish digestive tract. *Gastroenterology* 141, 197–207. <https://doi.org/10.1053/j.gastro.2011.03.042>.
20. Marjoram, L., Alvers, A., Deerhake, M.E., Bagwell, J., Mankiewicz, J., Cocchiari, J.L., Beerman, R.W., Willer, J., Sumigray, K.D., Katsanis, N., et al. (2015). Epigenetic control of intestinal barrier function and inflammation in zebrafish. *Proc. Natl. Acad. Sci. USA* 112, 2770–2775. <https://doi.org/10.1073/pnas.1424089112>.
21. Bojarczuk, A., Miller, K.A., Hotham, R., Lewis, A., Ogryzko, N.V., Kamuyango, A.A., Frost, H., Gibson, R.H., Stillman, E., May, R.C., et al. (2016). *Cryptococcus neoformans* Intracellular Proliferation and Capsule Size Determines Early Macrophage Control of Infection. *Sci. Rep.* 6, 21489. <https://doi.org/10.1038/srep21489>.
22. Nguyen-Chi, M., Laplace-Builhe, B., Travnickova, J., Luz-Crawford, P., Tejedor, G., Phan, Q.T., Duroux-Richard, I., Levraud, J.P., Kissa, K., Lutfalla, G., et al. (2015). Identification of polarized macrophage subsets in zebrafish. *Elife* 4, e07288. <https://doi.org/10.7554/eLife.07288>.
23. López-Muñoz, A., Sepulcre, M.P., Roca, F.J., Figueras, A., Meseguer, J., and Mulero, V. (2011). Evolutionary conserved pro-inflammatory and antigen presentation functions of zebrafish IFN γ revealed by transcriptomic and functional analysis. *Mol. Immunol.* 48, 1073–1083. <https://doi.org/10.1016/j.molimm.2011.01.015>.
24. Gosain, A., and DiPietro, L.A. (2004). Aging and wound healing. *World J. Surg.* 28, 321–326. <https://doi.org/10.1007/s00268-003-7397-6>.
25. Naomi, R., Bahari, H., Yazid, M.D., Embong, H., and Othman, F. (2021). Zebrafish as a Model System to Study the Mechanism of Cutaneous Wound Healing and Drug Discovery: Advantages and Challenges. *Pharmaceuticals* 14, 1058. <https://doi.org/10.3390/ph14101058>.
26. Dai, J., Shen, J., Chai, Y., and Chen, H. (2021). IL-1 β Impaired Diabetic Wound Healing by Regulating MMP-2 and MMP-9 through the p38 Pathway. *Mediators Inflamm.* 2021, 6645766. <https://doi.org/10.1155/2021/6645766>.
27. Mirza, R.E., Fang, M.M., Ennis, W.J., and Koh, T.J. (2013). Blocking interleukin-1 β induces a healing-associated wound macrophage phenotype and improves healing in type 2 diabetes. *Diabetes* 62, 2579–2587. <https://doi.org/10.2337/db12-1450>.
28. Holl, J., Kowalewski, C., Zimek, Z., Fiedor, P., Kaminski, A., Oldak, T., Moniuszko, M., and Eljaszewicz, A. (2021). Chronic Diabetic Wounds and Their Treatment with Skin Substitutes. *Cells* 10, 655. <https://doi.org/10.3390/cells10030655>.
29. Nair, S., Huynh, J.P., Lampropoulou, V., Loginicheva, E., Esaurova, E., Gounder, A.P., Boon, A.C.M., Schwarzkopf, E.A., Bradstreet, T.R., Edelson, B.T., et al. (2018). *Irg1* expression in myeloid cells prevents immunopathology during *M. tuberculosis* infection. *J. Exp. Med.* 215, 1035–1045. <https://doi.org/10.1084/jem.20180118>.
30. Tomlinson, K.L., Riquelme, S.A., Baskota, S.U., Drić, M., Monk, I.R., Stinear, T.P., Lewis, I.A., and Prince, A.S. (2023). *Staphylococcus aureus* stimulates neutrophil itaconate production that suppresses the

- oxidative burst. *Cell Rep.* 42, 112064. <https://doi.org/10.1016/j.celrep.2023.112064>.
31. Negut, I., Grumezescu, V., and Grumezescu, A.M. (2018). Treatment Strategies for Infected Wounds. *Molecules* 23, 2392. <https://doi.org/10.3390/molecules23092392>.
 32. Ye, S., Jiang, L., Wu, J., Su, C., Huang, C., Liu, X., and Shao, W. (2018). Flexible Amoxicillin-Grafted Bacterial Cellulose Sponges for Wound Dressing: In Vitro and in Vivo Evaluation. *ACS Appl. Mater. Interfaces* 10, 5862–5870. <https://doi.org/10.1021/acsami.7b16680>.
 33. Rădulescu, M., Holban, A.M., Mogoantă, L., Bălășeanu, T.A., Mogoșanu, G.D., Savu, D., Popescu, R.C., Fufă, O., Grumezescu, A.M., Bezirtzoglou, E., et al. (2016). Fabrication, Characterization, and Evaluation of Bionanocomposites Based on Natural Polymers and Antibiotics for Wound Healing Applications. *Molecules* 21, 761. <https://doi.org/10.3390/molecules21060761>.
 34. Mirhaj, M., Labbaf, S., Tavakoli, M., and Seifalian, A. (2022). An Overview on the Recent Advances in the Treatment of Infected Wounds: Antibacterial Wound Dressings. *Macromol. Biosci.* 22, e2200014. <https://doi.org/10.1002/mabi.202200014>.
 35. Seidelman, J., and Anderson, D.J. (2021). Surgical Site Infections. *Infect. Dis. Clin. North Am.* 35, 901–929. <https://doi.org/10.1016/j.idc.2021.07.006>.
 36. Miskolci, V., Tweed, K.E., Lasarev, M.R., Britt, E.C., Walsh, A.J., Zimmerman, L.J., McDougal, C.E., Cronan, M.R., Fan, J., Sauer, J.D., et al. (2022). In vivo fluorescence lifetime imaging of macrophage intracellular metabolism during wound responses in zebrafish. *Elife* 11, e66080. <https://doi.org/10.7554/eLife.66080>.
 37. Edman, D.C., Pollock, M.B., and Hall, E.R. (1968). *Listeria monocytogenes* L forms. I. Induction maintenance, and biological characteristics. *J. Bacteriol.* 96, 352–357. <https://doi.org/10.1128/jb.96.2.352-357.1968>.
 38. Tsarouchas, T.M., Wehner, D., Cavone, L., Munir, T., Keatinge, M., Lambertus, M., Underhill, A., Barrett, T., Kassapis, E., Ogryzko, N., et al. (2018). Dynamic control of proinflammatory cytokines IL-1 β and Tnf- α by macrophages in zebrafish spinal cord regeneration. *Nat. Commun.* 9, 4670. <https://doi.org/10.1038/s41467-018-07036-w>.
 39. Schindelin, J., Arganda-Carreras, I., Frise, E., Kaynig, V., Longair, M., Pietzsch, T., Preibisch, S., Rueden, C., Saalfeld, S., Schmid, B., et al. (2012). Fiji: an open-source platform for biological-image analysis. *Nat. Methods* 9, 676–682. <https://doi.org/10.1038/nmeth.2019>.
 40. Dobin, A., Davis, C.A., Schlesinger, F., Drenkow, J., Zaleski, C., Jha, S., Batut, P., Chaisson, M., and Gingeras, T.R. (2013). STAR: ultrafast universal RNA-seq aligner. *Bioinformatics* 29, 15–21. <https://doi.org/10.1093/bioinformatics/bts635>.
 41. Li, B., and Dewey, C.N. (2011). RSEM: accurate transcript quantification from RNA-Seq data with or without a reference genome. *BMC Bioinf.* 12, 323. <https://doi.org/10.1186/1471-2105-12-323>.
 42. Love, M.I., Huber, W., and Anders, S. (2014). Moderated estimation of fold change and dispersion for RNA-seq data with DESeq2. *Genome Biol.* 15, 550. <https://doi.org/10.1186/s13059-014-0550-8>.
 43. GTEx Consortium (2017). Genetic effects on gene expression across human tissues. *Nature* 550, 204–213. Erratum in: *Nature*. 2017 Dec 20. <https://doi.org/10.1038/nature24277>.

STAR★METHODS

KEY RESOURCES TABLE

REAGENT or RESOURCE	SOURCE	IDENTIFIER
Bacterial and virus strains		
10403S, <i>L. monocytogenes</i> WT strain	Edman et al. ³⁷	N/A
10403S, <i>L. monocytogenes</i> WT strain-mCherry	Vincent et al. ¹⁵	N/A
10403S, Lm-Pyro	Sauer et al. ¹¹	N/A
10403S, Lm-Pyro mCherry	Vincent et al. ¹⁵	N/A
10403S, Δ hly	Jones and Portnoy ⁵	N/A
Chemicals, peptides, and recombinant proteins		
Phosphate buffered saline (PBS)	Sigma-Aldrich	Cat# P3813
TWEEN-20	Sigma	Cat# P1379
Difco Brain Heart Infusion (BHI)	Becton Dickinson	REF# 237500
streptomycin	Fisher	Cat#BP910-50
Agar	Fisher	Cat# BP1423
TRlzol	Ambion	Cat#15596-026
chloroform	Fisher	Cat#C298-500
anakinra	Kineret	CAS# 143090-92-0
ampicillin	thermofisher	Cat#BP176025
Critical commercial assays		
RNAqueous Micro Kit	Invitrogen	Cat# AM1931
SuperScript™ III First-Strand Synthesis System	Invitrogen	Cat# 18080051
FastStart Essential DNA Green Master	Roche	Cat# 6402712001
RNeasy Mini Kit	Qiagen	Cat#74104
OneStep RT-PCR Kit	Qiagen	Cat#210212
Deposited data		
RNA-seq data	This paper	GEO: GSE237265
Experimental models: Organisms/strains		
D. Rerio WT (AB)	ZIRC	ZL1
Zebrafish Tg(NF- κ B:GFP)	Kanther et al. ¹⁹	ZDB-TGCONSTRCT-120409-6
Zebrafish Tg(tnfa:GFP)	Marjoram et al. ²⁰	ZDB-TGCONSTRCT-150603-6
Zebrafish Tg(mpeg1.1:mCherry-CAAX)	Bojarczuk et al. ²¹	ZDB-TGCONSTRCT-160414-8
Oligonucleotides		
Forward primer for <i>il1b</i> qPCR: ATGGCGAACGTCATCCAAGA	Tsarouchas et al. ³⁸	N/A
Reverse primer for <i>il1b</i> qPCR: GAGACCCGCTGATCTCCTTG	Tsarouchas et al. ³⁸	N/A
Forward primer for <i>b-actin</i> qPCR: CACTGAGGCTCCCTGAATCCC	Tsarouchas et al. ³⁸	N/A
Reverse primer for <i>b-actin</i> qPCR: CGTACAGAGAGACAGCCTGG	Tsarouchas et al. ³⁸	N/A
<i>il1b</i> MO1 Sequence: CCCACAACTGCAAAATATCAGCTT	López-Muñoz et al. ²²	ZBD-MRPHLNO-110620-2
Standard control morpholino Sequence: CCTTACTCTCAGTTACAATTATA	Gene Tools	N/A
Forward primer for checking <i>il1b</i> MO altered splicing: ATGGCATGCGGGCAATATGAA	López-Muñoz et al. ²²	N/A
Reverse primer for checking <i>il1b</i> MO altered splicing: CACTCAGCTCTTGGATGA	López-Muñoz et al. ²²	N/A

(Continued on next page)

Continued

REAGENT or RESOURCE	SOURCE	IDENTIFIER
Recombinant DNA		
pPL2(mCherry)	Vincent et al. ¹⁵	N/A
pPL2e(pActA-mCherry)	Vincent et al. ¹⁵	N/A
Software and algorithms		
FIJI, Image J	Schindelin et al. ³⁹	RRID:SCR_002285
GraphPad Prism		RRID:SCR_002798
SAS		RRID:SCR_008567
Spliced Transcripts Alignment to a Reference (STAR)	Dobin et al. ⁴⁰	https://github.com/alexdobin/STAR
RSEM v1.3.3	Li and Dewey ⁴¹	https://deweylab.github.io/RSEM/
DESeq2 v1.32.0	Love et al. ⁴²	https://bioconductor.org/packages/release/bioc/html/DESeq2.html

RESOURCE AVAILABILITY

Lead contact

- Further information and requests for resources should be directed to and will be fulfilled by the lead contact, Anna Huttenlocher (huttenlocher@wisc.edu).

Materials availability

- This study did not generate new unique reagents.

Data and code availability

- Single-cell RNA-seq data have been deposited at GEO and are publicly available as of the date of publication. Accession numbers are listed in the [key resources table](#). Microscopy data reported in this paper will be shared by the [lead contact](#) upon request.
- This paper does not report original code.
- Any additional information required to reanalyze the data reported in this paper is available from the [lead contact](#) upon request.

EXPERIMENTAL MODEL AND STUDY PARTICIPANT DETAILS

Zebrafish Husbandry and Handling

All protocols using zebrafish in this study has been approved by the University of Wisconsin-Madison Research Animals Resource Center (protocol M005405-A02). Adult zebrafish were maintained on a 14 hr:10 hr light/dark schedule. Upon fertilization, embryos were transferred into E3 medium (4.96 μ M NaCl, 0.18 μ M KCl, 0.33 μ M CaCl₂*2H₂O, 0.4 μ M MgCl₂*6H₂O, 0.1% methylene blue) and maintained at 28.5°C. For wounding assays, 3 days post-fertilization (dpf) larvae were anesthetized in E3 medium containing 0.2 mg/mL Tricaine (ethyl 3-aminobenzoate; Sigma-Aldrich). Zebrafish strains utilized in this study are listed in the [key resources table](#). Larval zebrafish were used for all studies when sex cannot be determined.

Bacterial strains

Listeria monocytogenes strain 10403S was used in this study. Strains used in this study are listed in the [key resources table](#).

METHOD DETAILS

Zebrafish wounding and infection

To prepare bacteria for wound infection, a streak plate from *L. monocytogenes* strain 10403S frozen stock was grown at 37°C. A fresh colony was picked and grown statically in 1 mL brain–heart infusion (BHI) medium (Becton, Dickinson and Company, Sparks, MD) overnight at 30°C to reach stationary phase. Bacteria were sub-cultured for ~1.5–2 hr in fresh BHI (4:1, BHI:overnight culture) to achieve growth to mid-logarithmic phase (OD₆₀₀ \approx 0.6–0.8). 1 mL of the mid-logarithmic phase bacterial culture were spun down and washed three times in sterile phosphate buffered saline (PBS) and resuspended in 100 μ L of PBS. To infect and wound, zebrafish larvae were placed in 5 mL E3 medium containing Tricaine with 100 μ L bacterial resuspension and caudal fins of larvae were transected using surgical blade (Feather no. 10) at the tip of the notochord without injury to the notochord. For controls, uninfected wounds, 100 μ L sterile PBS was added in the medium instead of bacterial resuspension. After caudal fin transection, larvae were transferred to new tissue culture treated dishes and incubated for 1 hr on a horizontal

orbital shaker at gentle speed (75-100 rpm). Larvae were then rinsed with E3 medium and maintained at 28.5°C until fixed or CFU plating at indicated time points as described.

Fixation

Zebrafish larvae were fixed in 1.5% formaldehyde (Polysciences, Warrington, PA) containing 0.1 M Pipes (Sigma-Aldrich), 1.0 mM MgSO₄ (Sigma-Aldrich) and 2 mM EGTA (Sigma-Aldrich) at 4°C overnight. Samples were washed with PBS and stored in PBS at 4°C until imaging.

Tissue regrowth area measurement

Fixed larvae at indicated timepoints were placed in Ibidi chamber in 0.1% Tween-20-PBS solution. A single-plane brightfield image is acquired using Zeiss Zoomscope (EMS3/SyCoP3; Zeiss, Oberkochen, Germany; Plan-NeoFluar Z objective; 112X magnification (0.7 μm resolution, 2.1 mm field of view, 9 μm depth of field) and Zen software (Zeiss). Tissue regrowth area was measured using FIJI using the polygon tool by outlining the tail fin tissue area distal to the notochord.

NF-κB quantification

Tg(NFκB:EGFP) zebrafish larvae were fixed at indicated timepoints post wounding. Fixed larvae were placed in Ibidi chamber in 0.1% Tween-20-PBS solution and 5-micron step z-stack images were collected using spinning disk confocal microscope (CSU-X, Yokogawa, Sugar Land, TX) with a confocal scanhead on a Zeiss Observer Z.1 inverted microscope, a Photometrics Evolve EMCCD camera and Zen Software (Zeiss). To quantify NF-κB signal, collected images were analyzed using FIJI. Sum-projections of the z-stacks were generated and the integrated density of NF-κB GFP signal was quantified in the caudal fin tissue extending from the caudal vein loop to the wound edge excluding the notochord using polygon tool. To adjust for background variation in each larvae, a 48.7 x 48.7 micron box was drawn using the rectangle tool in FIJI and placed in region without NF-κB signal to measure integrated density within the box. Background integrated density was then subtracted. To account for differences in tail fin area, NF-κB index was calculated by normalizing NF-κB integrated density to regrowth area in each zebrafish.

Macrophage and TNFα expression quantification

Double transgenic lines (*Tg(tnfa:GFP)* × *Tg(mpeg1:mCherry-CAAX)* larvae were fixed at indicated timepoints post wounding. Fixed samples were placed in Ibidi chamber in 0.1% Tween-20-PBS solution and 5-micron step z-stack images were collected using spinning disk confocal microscope (CSU-X, Yokogawa, Sugar Land, TX) with a confocal scanhead on a Zeiss Observer Z.1 inverted microscope, a Photometrics Evolve EMCCD camera and Zen Software (Zeiss). Macrophage recruitment and TNFα expression in macrophages were quantified in the caudal fin tissue area distal to the caudal vein loop by area thresholding of fluorescence intensity using Fiji, as previously.³ Polygon tool was used to outline the area of measurement in the brightfield image of caudal fin and the outlined area was then copied onto the sum z-projection of the z-stack from the corresponding macrophage (mCherry) channel. Macrophage within the outlined area was measured after thresholding fluorescence intensity and the measured macrophage area was outlined using region of interest (ROI) manager and copied onto the sum z-projection of the z-stack from the corresponding TNFα channel. To measure TNFα within the outlined macrophage area, the ROI were copied onto the sum z-projection of the z-stack from the corresponding GFP channel and fluorescence intensity was thresholded. Percentage of macrophage area colocalized with TNFα was calculated. To account for differences in tail fin area, TNFα index was then computed by normalizing the percentage of TNFα+ macrophage to regrowth area in each zebrafish.

Bacterial burden quantification

To determine bacterial CFU counts, 10 zebrafish larvae were pooled from each treatment and each timepoint into 1.5 ml microcentrifuge tubes with 150 μl of 1x PBS. Pooled larvae were then homogenized using a mini bead beater for 15 seconds. Homogenates were subsequently serially diluted and plated on BHI agar containing 200 μg/mL streptomycin. Bacterial plates were incubated overnight at 37°C and CFUs were counted. To quantify bacterial burden using microscopy, mCherry-expressing WT *Lm* or *Lm*-Pyro were used, and infected larvae are fixed at indicated timepoints. Fixed samples were placed in Ibidi chamber in 0.1% Tween-20-PBS solution and 5-micron step z-stack images were collected using spinning disk confocal microscope (CSU-X, Yokogawa, Sugar Land, TX) with a confocal scanhead on a Zeiss Observer Z.1 inverted microscope, a Photometrics Evolve EMCCD camera and Zen Software (Zeiss). Fluorescent area of *Lm* at the tail fins was measured using area thresholding in FIJI.

RNA sequencing

At 24 hpw, tail fins of 50 larvae were pooled and collected in ice cold PBS for each condition in each biological replicate. RNA was extracted from pooled tail fins using TRIzol reagent and RNAqueous Micro Kit (Invitrogen). Extracted RNA was submitted to GENEWIZ™ for library preparation and sequencing. The pooled RNA libraries were sequenced on an Illumina HiSeq to obtain 150-bp paired-end reads.

RNA sequencing analysis

RNA-seq reads were aligned to zebrafish reference genome GRCz11 using STAR v2.7.8a⁴⁰ and the Ensembl release 95 transcript annotation. Default values were used for all STAR parameters except for `outFilterMismatchNoverLmax` (0.1), `outFilterScoreMinOverLread` (0.33), and

outFilterMatchNminOverLread (0.33), following the standardized pipeline established for the GTEx project.⁴³ Transcript abundance was quantified from the resulting alignments using RSEM v1.3.3⁴¹ and differential expression between conditions was assessed using DESeq2 v1.32.0.⁴²

RT-qPCR

At specified time points (1 dpw, 3 dpw, or 5 dpw), tail fins of 18 to 23 larvae were pooled and collected in ice cold PBS for each condition in each biological replicate. RNA was extracted from pooled tail fins using TRIzol reagent and RNAqueous Micro Kit (Invitrogen). cDNA was then synthesized using SuperScript III RT and oligo-dT (Invitrogen). Using cDNA as a template, quantitative PCR (qPCR) was performed using FastStart Essential DNA (Roche) and a LightCycler96 (Roche). Fold changes in *il1b* expression over unwound control condition at 1 dpw, normalized to *b-actin* were calculated from Cq values. Primers used for amplifying *il1b* and *b-actin* are listed in the [key resources table](#).

Morpholino injections

Morpholino oligonucleotides targeting splice sites between intron 2 and exon 3 of *il1b* were obtained from Gene Tools, OR.²² The second intron of *il1b* is retained causing a frame shift resulting in a premature stop codon. 3nL of 350 μ M *il1b* antisense oligonucleotides or std MO were injected into one-cell stage embryos. To test for morpholino knockdown efficiency, RNA from std MO or *il1b* MO injected larvae was extracted using RNeasy Mini Kit (Qiagen) and RT-PCR was performed using OneStep RT-PCR Kit (Qiagen) with primers listed in the [key resources table](#).

Drug treatment

For anakinra experiments, the zebrafish embryos were dechorionated at 1 dpf and E3 medium without methylene blue (E3-) was supplemented with 10 μ M anakinra (Kineret) and refreshed daily. For experiments depleting *Lm* infections, zebrafish E3- medium was supplemented with ampicillin (45 mg/ml, Fisher) and refreshed daily starting from 1 dpw, 2 dpw, or 3 dpw as indicated.

QUANTIFICATION AND STATISTICAL ANALYSIS

All experiments in the main figures in this study consist of at least three biological replicates and each biological replicate is defined as a separate clutch of larvae spawned on different days. All data were graphed using Prism (GraphPad Software, Inc, San Diego, CA) with statistical analysis performed using SAS/STAT 9.4 (SAS Institute Inc, Cary, NC). SAS proc mixed procedure was used for variance analysis to account for the variation due to fixed effects and random effects from samples, as previously.³ If the normality assumptions of errors failed, a non-parametric analysis was performed using the ranks. When rank analysis was performed, it is indicated in the figure legends. For RNA sequencing analysis, statistical testing for differential expression between each treatment group was performed using the Wald test implemented in the DESeq2 package and genes with a Benjamini–Hochberg corrected P value (FDR) \leq 0.05 were considered statistically significant. For RT-qPCRs, reactions were performed in three technical replicates and two-way ANOVA (Prism) was used to determine statistical significance by comparing the calculated Δ Cq derived from subtraction of cycle numbers for gene of interest from cycle numbers for housekeeping control gene. p values are displayed as * <0.05 , ** <0.01 , *** <0.001 and **** <0.0001 in the figures. Statistical details of experiments can be found in the figure legends.